Ab initio quantum–chemical computations of the electronic states in HgBr$_2$ and IBr: Molecules of interest on the Earth's atmosphere

Sebastian P. Sitkiewicz, Josep M. Oliva, Juan Z. Dávalos, Rafael Notario, Alfonso Saiz–Lopez, Diego R. Alcoba, Ofelia B. Oña, and Daniel Roca-Sanjuán

Ab initio quantum–chemical computations of the electronic states in HgBr$_2$ and IBr: Molecules of interest on the Earth's atmosphere

Sebastian P. Sitkiewicz,[1] Josep M. Oliva,[2] Juan Z. Dávalos,[2] Rafael Notario,[2] Alfonso Saiz–Lopez,[2] Diego R. Alcoba,[3,4] Ofelia B. Oña,[5] and Daniel Roca-Sanjuán[1,a)]

[1]*Institut de Ciència Molecular, Universitat de València, P.O. Box 22085, València 46071, Spain*
[2]*Department of Atmospheric Chemistry and Climate, Institute of Physical Chemistry Rocasolano, CSIC, Madrid 28006, Spain*
[3]*Departamento de Física, Facultad de Ciencias Exactas y Naturales, Universidad de Buenos Aires, Ciudad Universitaria, Buenos Aires 1428, Argentina*
[4]*Instituto de Física de Buenos Aires, Consejo Nacional de Investigaciones Científicas y Técnicas, Ciudad Universitaria, Buenos Aires 1428, Argentina*
[5]*Instituto de Investigaciones Fisicoquímicas Teóricas y Aplicadas, Universidad Nacional de La Plata, CCT La Plata, Consejo Nacional de Investigaciones Científicas y Técnicas, Diag. 113 y 64 (S/N), Sucursal 4, CC 16, La Plata 1900, Argentina*

The electronic states of atmospheric relevant molecules IBr and HgBr$_2$ are reported, within the UV-Vis spectrum range (170 nm $\leq \lambda_{photon} \leq$ 600 nm) by means of the complete–active–space self–consistent field/multi–state complete–active–space second–order perturbation theory/spin–orbit restricted–active–space state–interaction (CASSCF/MS–CASPT2/SO–RASSI) quantum–chemical approach and atomic–natural–orbital relativistic–correlation–consistent (ANO–RCC) basis sets. Several analyses of the methodology were carried out in order to reach converged results and therefore to establish a highly accurate level of theory. Good agreement is found with the experimental data with errors not higher than around 0.1 eV. The presented analyses shall allow upcoming studies aimed to accurately determine the absorption cross sections of interhalogen molecules and compounds with Hg that are relevant to better comprehend the photochemical processes taking place in the atmosphere. *Published by AIP Publishing.* [http://dx.doi.org/10.1063/1.4971856]

I. INTRODUCTION

For the past few decades, the phenomena that occur in the atmosphere have brought much more attention because of the increasing number of threats that weigh on our planet. Most of them come from the increased human activity in the industrial sector—the depletion of the ozone layer in the arctic regions, the oxidation of gaseous mercury and its further accumulation in snows—these are just the basic examples of them.[1,2] Most reactions that occur on the Earth's atmosphere involve photochemical processes driven by the absorptions within the UV–Vis spectrum which lead to highly reactive species (excited states of the compounds). Hence, knowledge of the nature of these excited species is relevant for a deeper understanding of the chemical evolution of the atmosphere.

Among the experimental and theoretical works carried out during the last decades on diatomic interhalogen molecules, IBr has been considered as one of the simplest models and therefore it has been extensively studied. The absorption spectrum of this molecule has been measured at 298 K by Seery and Britton.[3] Two bands appear in the spectrum with band maxima at 507 nm (2.44 eV) and 268 nm (4.62 eV).[3] The high–energy band is much weaker than the band appearing at the low–energy region of the spectrum, and slightly asymmetric. After deconvolution, the experimentalists pointed to the presence

of a third transition at 477 nm (2.60 eV), the origin of the asymmetry of the most intense band.[3] Furthermore, the spectroscopic properties of several low–lying electronic states, the ground state X $^1\Sigma^+$ and the excited spin–orbit (SO) states $1^3\Pi_2$, $1^3\Pi_1$, (2)0+, and (3)0+, were experimentally determined.[4–7] Regarding the theoretical studies, Pittner and Jungwirth[8] used the equation–of–motion coupled–cluster method with single and double excitations (EOM-CCSD) and spin–orbit multireference configuration interaction with single excitations (SO–MRCIS) to study the above mentioned low–lying SO states. The single–reference methodologies allowed for an accurate description around the wells of the bound states. However, this approach failed at larger bond lengths. Both Patchkovskii[9] and Li *et al.*[10] used high–accuracy MR methodologies to compute all the states of IBr that correlate to the four lowest dissociation limits. The features of the potential energy curves (PECs) along the bond stretching coordinate were determined including the avoided crossing points. Li *et al.*[10] also performed an exhaustive analysis of the spin–orbit coupling (SOC) effects and the contributions of the spin–free (SF) electronic states in the SO states. In such MR computations, CASSCF wavefunctions were computed with an active space including 4*p* and 5*p* shells of the Br and I atoms, respectively (10 active electrons in 6 active orbitals), and one in which the Br 4*d* shell is added (10 active electrons in 11 active orbitals). This level of theory gives rise to good agreements with the experimental data.[10] Nevertheless, it is worth considering the role of iodine 5*d* orbitals and therefore more symmetric active spaces.

a)E-mail: Daniel.Roca@uv.es

Regarding $HgBr_2$, we chose this molecule as representative for mercury compounds with great relevance in atmospheric chemistry.[11–13] The excited state properties of such molecules are basically unknown (as compared to the interhalogen systems) and it has become urgent to determine these properties in order to properly characterize the photochemical processes taking place in the atmosphere. Early experimental studies carried out at the end of the 1970s and the beginning of the 1980s measured the absorption spectrum of $HgBr_2$ at 473 and 442.5 K.[14,15] The study of Roxlo and Mandl[15] reported a high–intensity band with a maximum at 198 nm (6.26 eV) and a shoulder at around 204 nm (6.08 eV), and a lower–intensity broader band at low energies with a maximum at 224 nm (5.54 eV). In addition, a sharp band of medium intensity was reported at 183 nm (6.75 eV). So far, most of the theoretical studies for this compound and related mercury halides have been focused on the ground–state properties.[16–21] The only exception is the work of Wadt published in 1980.[22] In this study, the electronic structure of the low–lying excited states of $HgCl_2$ and $HgBr_2$ was determined on the basis of SF states computed by using a moderate-size CI method, named as POL(1) CI, and a double-zeta plus polarization quality basis set with effective core potentials (ECPs). The three absorption bands at 5.54, 6.26, and 6.75 eV were assigned to the $1^1\Pi_u$, $1^1\Sigma_u^+$, and $2^1\Sigma_u^+$ states, respectively. PECs were also computed by Wadt, showing that the first two states have bent equilibrium geometries, while the $2^1\Sigma_u^+$ state presents a linear structure. Unfortunately, in the work of Wadt, one of the key factors for heavy transition metal systems—spin–orbit coupling—was not computed. Moreover, the scalar relativistic effects were accounted for with approximated ECPs. Since the work of Wadt,[22] no further computational studies on the chemistry of the excited states in $HgBr_2$ have been reported.

In the present work, we use high–level multireference multiconfigurational methodologies in order to confirm previous assignments and to determine further aspects of the UV–Vis electronic spectra of IBr and $HgBr_2$ molecules. Our goal is also to establish a useful and highly accurate theoretical methodology able to predict the absorption cross sections of interhalogen and mercury–based systems of relevance in atmospheric chemistry, such as HgBr, HgBrOH, HgBrOBr, $HgCl_2$, and $HgBrNO_2$. Information about the photolytic properties of such molecules is key to assess their atmospheric lifetimes and in turn further understand the atmospheric cycle of halogens and mercury. Therefore, different methodological approaches which account for electron correlation and interaction between states are applied. In addition, besides presenting the computed electronic spectra, the discussion will be focused on the significance of additional issues required for establishing a correct methodology—the relativistic effects of core electrons in heavy elements (like bromine, iodine, and mercury) and the importance of accounting for spin–orbit coupling of states with different multiplicity, which has not been done in previous works for $HgBr_2$.

II. COMPUTATIONAL METHODS

The UV–Vis electronic spectra of IBr and $HgBr_2$ were determined in the present work with the multi–state CASPT2

(MS–CASPT2)[23] methodology, as implemented in the MOLCAS 7[24–26] and MOLCAS 8[27] programs, with four distinct basis sets for comparative purposes: two basis sets containing ECPs, Def2QZVP[28] and aug–cc–pVQZ–PP,[29–32] and two all–electron basis sets, Sapporo–DKH3–QZP–2012[33,34] (abbreviated Sapp–DKH3–QZP in this paper) and ANO–RCC–VQZP.[35] The latter is a generally contracted basis set while the others follow a specific contraction scheme. The number of contracted and primitive functions used in each basis set and the employed ECP are indicated as follows:

- **Def2QZVP**
  Hg: (9s,8p,7d,3f,1g) → [7s,5p,4d,3f,1g] + ECP–60.[28,36]
  Br: (24s,20p,10d,2f,1g) → [11s,7p,4d,2f,1g].[28]
  I: (17s,14p,11d,4f,1g) → [7s,6p,4d,4f,1g]
  + ECP–28.[28,32]

- **aug–cc–pVQZ-PP**
  Hg: (15s,12p,11d,4f,3g,2h) → [7s,7p,6d,4f,3g,2h]
  + ECP–60.[29,30]
  Br: (15s,12p,13d,3f,2g) → [7s,6p,5d,3f,2g]
  + ECP–10.[32]
  I: (15s,12p,13d,3f,2g) → [7s,7p,5d,3f,2g] + ECP–28.[32]

- **ANO–RCC-VQZP**[35]
  Hg: (25s,22p,16d,12f,4g,2h) → [9s,8p,6d,4f,3g,2h].
  Br: (20s,17p,11d,4f,2g) → [7s,6p,4d,2f,1g].
  I: (22s,19p,13d,5f,3g) → [8s,7p,5d,3f,2g].

- **Sapp–DKH3–QZP**
  Hg: (27s,22p,17d,11f,3g,3h) → [12s,10p,8d,5f,3g,2h].[34]
  Br: (22s,16p,12d,6f,5g,2h) → [10s,9p,8d,6f,4g,2h].[33]
  I: (25s,18p,14d,6f,5g,2h) → [11s,10p,8d,6f,4g,2h].[33]

The all–electron basis sets ANO–RCC–VQZP and Sapp–DKH3–QZP required the third–order Douglas–Kroll and Hess (DKH3) Hamiltonian[37–40] in order to account for the scalar relativistic effects of the inner electrons in Hg and I, whereas the basis sets containing ECPs, Def2QZVP, and aug–cc–pVQZ–PP were used with the standard Hamiltonian.

In the CASSCF computations, the C_{2v} and D_{2h} subgroups of the $C_{\infty v}$ and $D_{\infty h}$ symmetry point groups were used for IBr and $HgBr_2$, respectively. The correspondences of the irreducible representations (irreps) between C_{2v} and $C_{\infty v}$ point groups relevant to this work are $A_1 \rightarrow \Sigma^+$, $B_1 + B_2 \rightarrow \Pi$, $A_1 + A_2 \rightarrow \Delta$, and $A_2 \rightarrow \Sigma^-$. In the case of the D_{2h} and $D_{\infty h}$ point groups, the relevant correlating relationships are $A_g \rightarrow \Sigma_g^+$, $B_{1u} \rightarrow \Sigma_u^+$, $B_{1g} \rightarrow \Sigma_g^-$, $A_u \rightarrow \Sigma_u^-$, $B_{2g} + B_{3g} \rightarrow \Pi_g$, $B_{2u} + B_{3u} \rightarrow \Pi_u$, $A_g + B_{1g} \rightarrow \Delta_g$, and $A_u + B_{1u} \rightarrow \Delta_u$. In the computations, the mixing of the pertinent states was not allowed in order to correctly transform the irreps of the lower–symmetry groups to the infinite point groups.

Regarding the selection of the active spaces, several approaches were considered: recommendations from previous theoretical studies,[9,10] the occupation numbers of the quasi–canonical orbitals of initial MP2 computations, and the occupation numbers of the natural orbitals obtained in several test CASSCF computations with different active spaces. Based on the resulting information, a complete active space (CAS) of 10 electrons distributed in 13 orbitals was chosen for IBr (hereafter, CAS(10,13)), which is much larger

than that used in previous theoretical works. In the present study the CAS orbitals are σ_p and σ_p^* (I $5p_z \pm$ Br $4p_z$), 2 π_p and 2 π_p^* (I $5p_{x/y} \pm$ Br $4p_{x/y}$), 2 π_d (I $5d_{xz/yz} -$ Br $4d_{xz/yz}$), 2 δ and 2 δ^* (I $5d_{xy/x2-y2} \pm$ Br $4d_{xy/x2-y2}$), and σ_d (I $5d_{z2}$ + Br $4d_{z2}$), see Fig. 1. For HgBr$_2$, the CAS(12,12) was chosen and the performance was compared with that of a CAS(22,15). The former includes σ_g^+ and σ_g^{+*} (Br $4p_z \pm$ Hg $6s -$ Br $4p_z$), 2 π_u^{nb} and 2 $\pi_{g,p}^{nb}$ (Br $4p_{x/y} \pm$ Br $4p_{x/y}$), σ_u^{+nb} (Br $4p_z +$ Br $4p_z$), 2 π_u (Br $4d_{xz/yz} -$ Hg $6p_{x/y} -$ Br $4d_{xz/yz}$), σ_u^+ (Br $4d_{z2}$ + Hg $6p_z -$ Br $4d_{z2}$), and 2 $\pi_{g,d}^{nb}$ (Br $4d_{xz/yz} +$ Br $4d_{xz/yz}$), see Fig. 2, while the latter takes into account additional $5d$ occupied orbitals of mercury and lacks the last two nonbonding $\pi_{g,d}^{nb}$ molecular orbitals, which are shown to be irrelevant in the results with the smaller CAS. More details about the CAS selection and the nature of the natural orbitals shall be given in Sec. III. Note that for a balanced description of the atoms at the dissociation limit, the CAS should include non–truncated p and d shells. In this work, the aim is, however, to determine the electronic transitions at the ground–state equilibrium geometry and surrounding bound structures. Therefore, the CAS was chosen to be optimal in such region.

State–averaged CASSCF (SA–CASSCF) computations were carried out with the aforementioned CASs, with 6 averaged roots in each one of the irreps of the C$_{2v}$ point group (A$_1$, A$_2$, B$_1$, and B$_2$) for IBr and 8 averaged roots in all the irreps of the D$_{2h}$ point group (A$_g$, B$_{3u}$, B$_{2u}$, B$_{1g}$, B$_{1u}$, B$_{2g}$, B$_{3g}$, and A$_u$) in the case of HgBr$_2$. The same number of singlet and triplet states is considered in the quantum–chemical computations. Hence, the total number of electronic states are 24 singlet states and 24 triplet states for IBr and 64 singlet states and 64 triplet states for HgBr$_2$. A different number of averaged roots was also tested in order to analyze the effect of
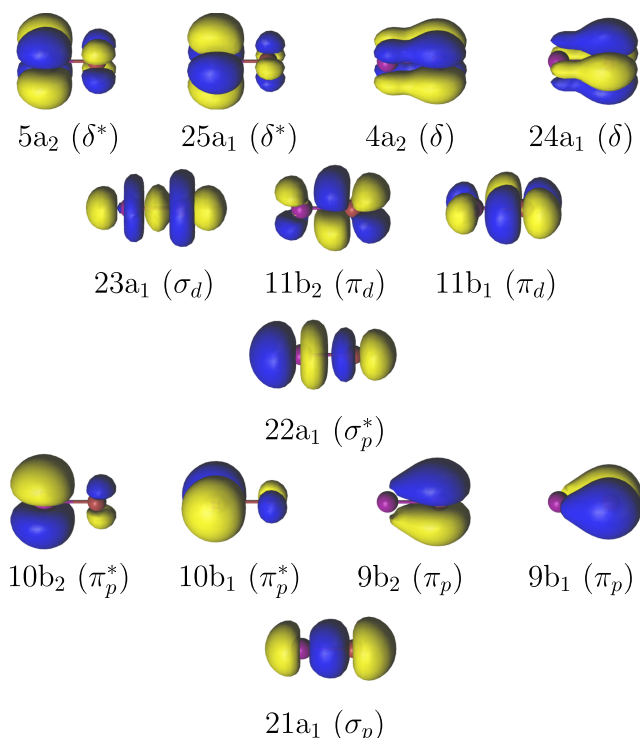

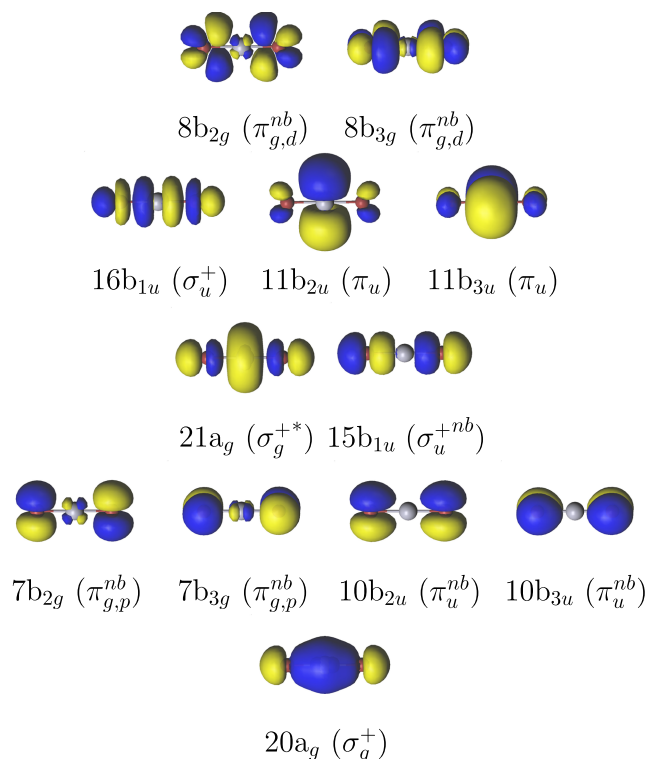FIG. 1. Selected CAS(10,13) orbitals for the CASSCF/MS–CASPT2 computations of IBr.

FIG. 2. Selected CAS(12,12) orbitals for the CASSCF/MS–CASPT2 computations of HgBr$_2$.

considering higher–energy states. In particular, 4 and 8 roots were tested for IBr and 5 and 11 roots in the case of HgBr$_2$.

Dynamic electron correlation was computed with the CASPT2[41–43] method. In order to minimize the effect of intruder states, the imaginary level shift was used with a value of 0.2 a.u.[44] Two values of the ionization potential electron affinity (IPEA) shift were tested, 0.00 and 0.25 a.u.[43] The latter was proposed by Ghigo, Roos, and Malmqvist in order to correct the systematic errors found in the energy differences between closed– and open–shell situations. The interaction of the CASPT2 states between themselves was subsequently evaluated with the MS–CASPT2 method. In particular, perturbed wavefunctions at MS–CASPT2 level were projected onto the space spanned by the original CASSCF functions. The final MS–CASPT2 wavefunction of state p can be written as[23]

$$\Psi_p = \sum_\alpha C_{p\alpha} \mid \alpha \rangle + \chi_p, \tag{1}$$

where α are the CASSCF reference functions of the SF states, and χ_p is the first–order perturbation for the new state p.

Since the studied molecules contain heavy atoms, for the all–electron basis sets the scalar relativistic effect was taken into account by the third–order Douglas–Kroll and Hess approach.[37–40] The SOC effect was computed with the restricted–active–space state–interaction (RASSI) method using the atomic mean–field approximation (AMFI).[45] The SO eigenstates were obtained by diagonalizing the electronic (el) and SO Hamiltonians, $H_{el} +$ H$_{SO}$, in the basis of the SF eigenfunctions of the H$_{el}$.[46] CASSCF spin–free wavefunctions were used in the computations of the SO states with the single–state CASPT2 (SS–CASPT2) method, whereas the determination

of the SO states with the MS–CASPT2 method was carried out with correlated wavefunctions (Eq. (1)).

The oscillator strength (f) was computed with the following formula:

$$f = \frac{2}{3}\Delta E \, |TDM|^2, \tag{2}$$

where ΔE stands for the SS– or MS–CASPT2 vertical excitation energies (VEEs). The TDM refers to the transition dipole moment, $TDM = \langle g \mid \mu \mid f \rangle$, between the initial (g) and final (f) electronic SF or SO states, and μ is the dipole moment operator.

Ground–state equilibrium geometries were optimized at the same level of theory as that used for the computation of the VEEs (i.e., MS–CASPT2 method and the distinct basis sets) and imposing the constraints of the C_{2v} and D_{2h} symmetry point groups for IBr and $HgBr_2$, respectively. Equilibrium geometries of the excited SF states in IBr were subsequently determined, as energy minima, at the MS(NRoots = 6)–CASPT2(10,13)–IPEA(0.25 a.u.)/ANO–RCC–VQZP level of theory also with the C_{2v} symmetry constraint. The obtained IBr bond lengths (R_{IBr}) and the computed adiabatic energies (T_e) were compared with the experimental data from the gas phase[5,7,47–50] and previous MR results.[9,10] For $HgBr_2$, the geometries of the relevant low–lying SF states were optimized at the MS(NRoots = 5)–CASPT2(12,10)–IPEA(0.25 a.u.)/ANO–RCC–VQZP level. The symmetry constraint was here reduced to the C_{2v} symmetry point group to allow bent structures, which were previously obtained by Wadt.[22] Since the $8b_{2g}$ ($\pi_{g,d}^{nb}$) and $8b_{3g}$ ($\pi_{g,d}^{nb}$) unoccupied orbitals (see Figure 2) are not relevant in these states, they were kept as secondary orbitals. The decrease of active orbitals and number of roots allowed a reduction of the computational effort required to determine the numerical gradients at the MS–CASPT2 level. Furthermore, all the obtained minima were characterized by computing the frequencies using the harmonic approximation. In these computations, the symmetry was lowered to the C_s point group to obtain information about the three normal modes of the molecule, symmetric (ν_{sym}) and asymmetric (ν_{asym}) stretching and bending (ν_{bend}).

III. RESULTS AND DISCUSSION

In this section, the benchmark for IBr is first discussed. In this molecule, several theoretical and experimental data have been previously reported in the literature for the ground and

excited states and therefore comparison with those studies will allow establishing an accurate methodology for determining UV–Vis electronic spectra of compounds with heavy halogen atoms. Next, the findings for the $HgBr_2$ compound are presented and analyzed, taking also into account the experience and knowledge acquired in the calibrations carried out in IBr. In each section, the performance of distinct basis sets and the SOC effects are first discussed. Second, issues related to the active space and the number of SA states in the CASSCF computations are considered. Third, the IPEA shifts (0.00 vs 0.25 a.u.) and SS vs MS approaches of the CASPT2 method are compared. Finally, on the basis of the findings obtained with the methodology established as accurate, the nature of the transitions is given together with the interpretation of the absorption spectra measured in the experiments and information about the excited–state equilibrium structures.

A. IBr

The results obtained for the ground–state equilibrium geometry, the VEEs between singlet SF electronic states, and the associated f with the four distinct basis sets are compiled in Table I. Despite the distinct manners of accounting for scalar relativistic effects, the Def2QZVP, aug–cc–pVQZ–PP, ANO–RCC–VQZP, and Sapp–DKH3–QZP basis sets give rise to values of the bond distance R_{IBr} close to the experimental value ($R_{IBr} = 2.469$ Å).[47] The highest deviation takes place in the aug–cc–pVQZ–PP basis set, although with a small difference of 0.009 Å.

The deconvolution of the spectrum of IBr gives rise to three transitions at 2.44, 2.60, and 4.62 eV.[3] Without taking into account the SOC, for the allowed singlet–singlet transitions, the four computational procedures used in this work produce very similar results with energy deviations of the positions of the maxima not higher than 0.16 eV (Table I). However, only two significant transitions are computed, $1^1\Sigma^+ \rightarrow 1^1\Pi$ and $1^1\Sigma^+ \rightarrow 2^1\Pi$, which appear in the region of the experimental band maxima at 2.60 and 4.62 eV, while the lowest–energy transition obtained experimentally at 2.44 eV is missing in this description provided by the singlet SF electronic states. As analyzed in detail in previous works by Patchkovskii[9] and Li *et al.*,[10] strong SOC takes place in this molecule. It implies the mixing of singlet and triplet states, which gives rise to transitions contributing in the low–energy region of the absorption spectrum.

TABLE I. Ground–state equilibrium bond lengths (R_{IBr}) and main vertical excitation energies (VEEs) in eV and associated oscillator strength (f) values (within parentheses) obtained for IBr from the computation of the SF states (SOC not considered) with the MS–CASPT2(10,13)–IPEA(0.25 a.u.) methodology and different basis sets. Experimental data included for comparison.

Basis set	Def2QZVP	aug–cc–pVQZ–PP	ANO–RCC–VQZP	Sapp–DKH3–QZP	Expt.
R_{IBr} (Å)	2.467	2.460	2.473	2.472	2.469[47]
SF[a] state					
...	...	...	...	...	2.44[b]
$1^1\Pi$	2.51 (0.000 29)	2.61 (0.000 04)	2.56 (0.000 28)	2.44 (0.000 04)	2.60[3]
$2^1\Pi$	4.43 (0.000 80)	4.59 (0.000 96)	4.46 (0.000 93)	4.33 (0.000 97)	4.62[3]
$2^1\Sigma^+$	5.48 (0.000 40)	5.62 (0.000 44)	5.45 (0.000 30)	5.44 (0.000 27)	

[a]Spin–free.
[b]Band not found with the methodology presented in this table.

TABLE II. Main vertical excitation energies (VEEs) in eV and associated oscillator strength (f) values (within parentheses) obtained for IBr from the computation of the SO states with the SOC–MS–CASPT2(10,13)–IPEA(0.25 a.u.) methodology and distinct basis sets. Experimental data included for comparison.

Basis set SO[a] state		Def2QZVP	aug–cc–pVQZ–PP	ANO–RCC–VQZP	Sapp–DKH3–QZP	Expt.[3]
(1)1	$(1^3\Pi_1)$	2.06 (4.3×10^{-6})	2.11 (7.0×10^{-8})	2.01 (0.000 03)	1.89 (2.7×10^{-5})	
(2)0_+	$(1^3\Pi_{0+})$	2.11 (0.000 11)	2.11 (2.0×10^{-6})	2.39 (0.001 87)	2.27 (0.001 75)	2.44
(2)1	$(1^1\Pi_1)$	2.52 (0.000 28)	2.61 (0.000 04)	2.65 (0.000 25)	2.54 (0.000 03)	2.60
(3)1	$(2^3\Pi_1)$	4.18 (0.000 04)	4.31 (1.0×10^{-6})	4.13 (0.000 21)	4.01 (0.000 21)	
(3)0_+	$(2^3\Pi_{0+})$	4.28 (0.000 92)	4.32 (4.0×10^{-6})	4.42 (0.000 10)	4.30 (0.000 27)	
(4)1	$(2^1\Pi_1)$	4.44 (0.000 74)	4.59 (0.000 96)	4.57 (0.000 70)	4.45 (0.000 78)	4.62
(4)0_+	$(1^3\Sigma_{0+}^-)$	4.88 (1.0×10^{-7})	4.95 (1.0×10^{-7})	4.70 (0.000 20)	4.70 (0.000 22)	
(5)1	$(1^3\Sigma_1^-)$	4.88 (3.0×10^{-6})	4.95 (0.5×10^{-7})	4.95 (0.000 04)	4.94 (0.000 01)	
(6)1	$(1^3\Sigma_1^+)$	5.00 (0.000 03)	5.06 (1.0×10^{-7})	5.08 (2.7×10^{-6})	5.03 (8.0×10^{-5})	
(5)0_+	$(2^1\Sigma_{0+}^+)$	5.51 (0.000 46)	5.62 (0.000 44)	5.75 (5.0×10^{-6})	5.74 (0.000 07)	

[a]Spin–orbit.

Table II compiles the VEEs and f for the transitions based on SO states. Similarly to other authors,[10] we used here two distinct nomenclatures to label the SO states. In one of them, the SF state that mostly contributes to the SO state is written together with the Ω value given as a subindex (for example, the SO state arising mainly from the $2^1\Pi$ SF state and with Ω value of 1 is represented in this nomenclature by $2^1\Pi_1$). This nomenclature contains information about the SF states. However, it is not accurate when several SF states contribute to the SO state with similar percentages. In this case, another nomenclature in which the states with different Ω values are ordered by their energies might be more precise (for example, the same SO state used above, which is the fourth state with Ω value of 1, is represented here by (4)1). As can be seen in Table II, the SO state (4)1–$(2^1\Pi_1)$ is mainly responsible for the experimental band with a maximum at 4.62 eV. In the case of the basis sets with ECPs, the VEE and f values do not change with respect to the data corresponding to the SF state $2^1\Pi$ from Table I. Thus, the transition is not affected by the SOC in the results obtained with those basis sets. This is due to the fact that with the Def2QZVP and aug–cc–pVQZ–PP basis sets this band basically corresponds to a pure singlet–singlet transition. On the contrary, the transition is displaced from 4.46 to 4.57 eV for the ANO–RCC–VQZP and from 4.33 to 4.45 eV for the Sapp–DKH3–QZP, approaching therefore the experimental value of 4.62 eV. The reason for this displacement is that, in the all–electron basis sets, the corresponding SO state is formed by a significant contribution of the formally forbidden triplet $1^3\Sigma^-$ state. This remarkable difference points to a poor description of the basis sets with ECPs, in which the H_{SO} is only applied to the valence electrons.

More discrepancies also appear in the determination of the low–energy transitions. Thus, when taking into account the SOC, the transition at 2.52 eV (for Def2QZVP) and 2.61 eV (for aug–cc–pVQZ–PP) is maintained as a pure spin transition. Several other transitions arise in the scenario provided by the SO states. However, their associated oscillator strength is insignificant. Hence, in the view of basis sets with ECP, the experimental signal at 2.44 eV is still missing. On the contrary, the findings obtained with the all–electron basis sets show a transition at 2.39 eV (ANO–RCC–VQZP) and 2.27 eV

(Sapp–DKH3–QZP), arising from the population transfer from the ground state (which already has some triplet contribution) to the $(2)0_+$ SO state mainly formed by the $1^3\Pi$ triplet SF state. This is in agreement with the findings obtained by Patchkovskii[9] and Li *et al.*[10]

It is demonstrated here that a methodology taking into account both the SOC and all–electron basis is required for describing the lowest–energy band of the absorption spectrum of IBr. Both the ANO–RCC–VQZP and Sapp–DKH3–QZP basis sets provide good agreement with experiments with deviations lower than 0.1 eV. Nevertheless, considering the fact that the Sapporo basis set requires higher computational resources, the ANO basis set can be chosen as the most efficient one. Therefore, we used this basis set for the subsequent calibrations of the methodology, which are discussed below.

Previous studies at the MRQDPT2[51,52] level have been performed with CAS(10,6) and CAS(10,11).[9] In this work, we used a larger CAS, which also includes the antibonding δ^* molecular orbitals (MOs) ($25a_1$ and $5a_2$) in order to decrease the imparity in the selection of d-type atomic orbitals (AOs) of bromine and not iodine. The effect of including higher excited states and their possible influence on the wavefunction of lower–energy states was also analyzed. The convergence of the obtained VEEs and the corresponding f values was tested at the MS–CASPT2(10,13)/ANO–RCC-VQZP level of theory for 4, 6, and 8 roots for each symmetry (see Table S.I, supplementary material). The differences between the transition energies do not exceed 0.13 eV, which is a small enough error for our purposes. Including a very large number of roots per symmetry might not be suitable for the description of the high–energy states, if the CAS is not enlarged, since other d orbitals might contribute to these high states. The amount of 6 roots seems appropriate for an accurate description of the UV-Vis region of the spectrum reported in the experimental studies.[3]

Turning now to the calibrations of the methodologies including dynamic electron correlation (CASPT2), the IPEA shift of 0.25 a.u. systematically increases the VEEs by around 0.2 eV approaching the experimental data (Table S.II, supplementary material). Hence, the IPEA correction is necessary when large basis sets are employed in the computations. On the other hand, comparison of the SS– and MS–CASPT2
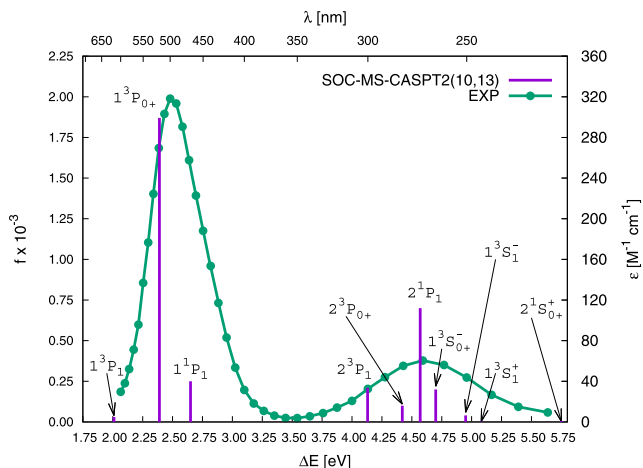
FIG. 3. Graphical representation of the vertical excitation energies (VEEs) in eV (ΔE) and nm (λ) and associated f for the SO states of IBr computed at the MS–CASPT2(10,13)–IPEA(0.25 a.u.)/ANO–RCC–VQZP level (purple, sticks), and the experimental molar extinction coefficients ε (dark green line, circles).[3]

methods (Table S.III, supplementary material) shows that the same energy values are obtained with both approaches. The absolute values for corresponding f are different although they maintain the relative magnitude for the transitions. As previously stated by Lindh *et al.*,[53] this agreement between the SS and MS approaches points to an accurate determination of the dynamical electron correlation with the perturbation theory, with no unphysical values derived by the symmetrization procedure carried out in the MS computation.

Taking into account the data of the experimental cross sections,[3] the previous theoretical determinations of the PECs of IBr,[9,10] and the above test computations, it can be concluded that an accurate level of theory for characterizing the low–lying excited states of IBr corresponds to the SOC–MS–CASPT2/ANO–RCC–VQZP level with a CAS(10,13) and 6 averaged states to generate the multiconfigurational wavefunction and an IPEA shift value of 0.25 a.u.

Fig. 3 displays the experimental absorption spectrum together with the predicted quantum–chemical electronic spectrum at the SOC–MS–CASPT2/ANO–RCC–VQZP level. The present results support the previous theoretical findings.[9,10] In those studies, the authors computed the PECs along the dissociation coordinate and analyzed the correlation of the low–lying Ω states with the atomic states of I and Br.

We refer the reader to such works for a detailed interpretation of the cross sections and the description of the nature of the excitations. In the following, we shall only focus on aspects which allow to calibrate the computational strategy used here to determine the excited–state equilibrium geometries and the corresponding electronic band origins (T_e). As described in Sec. II, the computational approach of this work implies geometry optimizations of the SF states based on MS–CASPT2 numerical gradients and energy computations of the SO states at the optimized geometries.

Taking into account the electronic configurations (Table S.IV, supplementary material) and the contribution of the SF states into the final SO states (Table S.V, supplementary material), the band peaking at 4.57 eV, which can be mainly assigned to the 4(1) SO state, arises from the singlet $2^1\Pi$ (72%) and the triplet $2^3\Pi$ (23%). These SF states correspond to excitations from the π_p bonding to the σ_p^* anti–bonding orbitals (see also the work by Li *et al.*).[10] This implies that the bonding interaction between the I and Br atoms becomes weak in the 4(1) state and its population brings the molecule to dissociation, as confirmed by the MS–CASPT2 geometry optimization of the singlet $2^1\Pi$ electronic SF state.

Regarding the transition at 2.65 eV, which is related to the (2)1 SO state, it originates mainly from the singlet $1^1\Pi$ SF state, which implies an electron promoted from a π_p^* to the σ_p^* orbital. In this case both orbitals are anti–bonding and the population of this state does not dissociate the molecule, which is confirmed by the MS–CASPT2 geometry optimization. The equilibrium geometry for this state is $R_{IBr} = 2.879$ Å, much longer than the ground–state optimized bond distance, $R_{IBr} = 2.473$ Å (see Table III). This is due to the stronger anti–bonding character of the σ_p^* molecular orbitals (MOs) as compared to that of the π_p^* MOs.

Finally, the lowest–energy experimental transition at 2.4 eV can be ascribed to the $1^3\Pi$ SF state. This state is also formed by π_p^* to σ_p^* electron promotion as for the $1^1\Pi$. Consequently, the MS–CASPT2 optimized geometry, $R_{IBr} = 2.795$ Å, is close to the value for the $1^1\Pi$ minimum, 2.879 Å, and higher than the ground-state equilibrium bond length, 2.473 Å (see Table III). Patchkovskii[9] and Li *et al.*[10] also found that the SO states originated by the SF state ($1^3\Pi_2$, $1^3\Pi_1$, and $1^3\Pi_{0+}$) are bound states with geometries in qualitative agreement with those reported here. In summary, in the present and previous theoretical works,[9,10] an increase of the IBr bond length

TABLE III. Equilibrium bond lengths (R_{IBr}, in Å) and adiabatic transition energies (T_e, in eV) of IBr obtained for several low–lying SO states with the SOC–MS(NRoots = 6)–CASPT2(10,13)–IPEA(0.25 a.u.)/ANO-RCC–VQZP methodology used here, other levels of theory from the literature, and from the experiments.

SO[a] state		MS–CASPT2(10,13)		MRQDPT2(10,11)[9]		MRCI + Q[10]		Expt.	
		T_e	R_{IBr}	T_e	R_{IBr}	T_e	R_{IBr}	T_e	R_{IBr}
(1)0$_+$	($1^1\Sigma_{0+}^+$)	0.00	2.473	0.00	2.514	0.00	2.482	0.00	2.469[47]
(1)2	($1^3\Pi_2$)	1.31	2.795[b]	1.34	2.849	1.42	2.863	1.42[7,48]	2.842[48]
(1)1	($1^3\Pi_1$)	1.43	2.795[b]	1.46	2.876	1.55	2.899	1.53[5,49]	2.858[49]
(1)0$_-$	($1^3\Pi_{0-}$)	1.68	2.795[b]	1.70	3.032				
(2)0$_+$	($1^3\Pi_{0+}$)	1.83	2.795[b]	1.91	2.853	2.05	2.898	2.00[50]	2.83[50]
(2)1	($1^1\Pi_1$)	1.92	2.879						

[a]Spin–orbit.
[b]Geometry of spin–free $1^3\Pi$ state.

of around 0.3 Å is obtained between the equilibrium structures of the ground state and the SO states originated from the $1^3\Pi$ SF state, similarly to the data reported in the experimental studies,[47–50] as shown in Table III.

The adiabatic energies (T_e) obtained in this work for the SO states mentioned in the previous paragraph, 1.31 eV, 1.43 eV, and 1.83 eV, respectively, are also close to those determined by Patchkovskii,[9] despite the use of a distinct methodology. In particular, Patchkovskii used CAS(10,6) and CAS(10,11) wavefunctions and the MRQDPT2 method to account for the dynamic electron correlation.[9] The largest deviation is 0.08 eV. Higher differences are found with respect to the MRCI + Q results[10] and the experimental data.[5,7,48–50] Nevertheless, they are still small with an average deviation of 0.13 eV with respect to the experimental data. Note that the determination of R_{IBr} and T_e of Patchkovskii[9] and Li *et al.*[10] was based on the exploration of the PEC along the stretching of the bond and using the energies of the SO states, while in the present study the minima are found by computing the numerical gradient of the SF electronic states, and next T_e energies are determined by computing the SO states at each optimized geometry (of the SF states). The agreement with the values from Patchkovskii[9] and Li *et al.*[10] allows to conclude that our computational strategy is accurate enough and would be much more efficient for upcoming studies on molecules with more degrees of freedom in which a full exploration of the PECs would be prohibitive.

B. HgBr$_2$

Table IV compiles the data related to the ground–state equilibrium geometry, VEEs between singlet SF electronic states, and associated f computed in this work and also obtained in previous theoretical and experimental studies.[14,15,22,54,55] For the ground–state equilibrium structure, experimental studies do not give a definitive answer about the optimal R_{HgBr} bond length for gaseous mercury bromide.[21] Akishin and Spiridonov[55] reported a value of 2.41 Å, which was used by Wadt to theoretically determine the electronic structure of the low–lying electronic states. However, in the review of Hargittai,[54] a linear geometry with a mercury–bromine distance of $R_{HgBr} = 2.374$ Å (obtained from thermal averages) was proposed as the best estimation. Regarding theoretical studies, several works have focused only on the determination of the ground–state geometry. From the most recent papers, the work of Kim *et al.*[20] consists of benchmark computations with a large number of density functional theory (DFT) functionals and their performance in determining equilibrium geometries for a large set of mercury halides. In the case of HgBr$_2$, among the tested functionals, the PBE0 with aug–cc–pVTZ–PP basis set gave the closest results to the experiment in determining geometry and harmonic vibrational frequencies $\left(R_{HgBr}^{PBE0} = 2.392\text{ Å}\right)$. In another work, Balabanov and Peterson[21] performed a detailed study of the ground state structure and the vibrational levels of the mercury halides, HgCl$_2$, HgBr$_2$, and HgBrCl, using a high–level *ab initio* CCSD(T) methodology and aug–cc–pVXZ–PP basis sets. These previous publications explored the effect of basis sets, SOC, scalar relativity (SR) effects, and core–valence correlation (CV) on the quality of the obtained ground–state structures. For all the studied covalent mercury halides, they confirmed linear structures of the molecules.

TABLE IV. Ground–state equilibrium bond lengths (R_{HgBr}), main vertical excitation energies (VEEs) in eV and associated oscillator strength (f) values (within parentheses) obtained for HgBr$_2$ from the computation of the SF states (SOC not considered) with the MS–CASPT2(12,12)–IPEA(0.25 a.u.) methodology and distinct basis sets. Experimental data included for comparison.

Basis set	Def2QZVP	aug–cc–pVQZ–PP	ANO–RCC–VQZP	Sapp–DKH3–QZP	POL(1) CI[22]	Expt.
R_{HgBr} (Å)	2.364	2.338	2.363	2.365	2.410	2.374[54]
SF[a] state						
$1^3\Pi_g$	4.59	4.64	4.56	4.58	4.00	
$1^1\Pi_g$	4.80	4.90	4.75	4.76	4.29	
$1^3\Pi_u$	5.23	5.34	5.17	5.19	4.35	
$1^1\Pi_u$	5.41 (0.027 12)	5.49 (0.030 60)	5.34 (0.029 03)	5.39 (0.022 15)	4.72 (0.023 90)	5.54,[15] 5.39[14]
$1^3\Sigma_u^+$	5.49	5.61	5.46	5.49	4.57	
$1^1\Sigma_u^+$	6.44 (0.104 28)	6.37 (0.059 25)	6.35 (0.116 13)	6.35 (0.094 75)	5.97 (0.232 00)	6.26,[15] 6.36[14]
$2^3\Sigma_u^+$	6.54	6.47	6.47	6.49	6.33	
$1^3\Delta_u$	6.69	6.59	6.61	6.57	6.47	
$1^1\Delta_u$	6.70	6.58	6.63	6.59	6.50	
$1^1\Sigma_u^-$	6.77	6.62	6.69	6.67	6.63	
$1^3\Sigma_g^+$	6.78	6.78	6.70	6.67		
$1^3\Sigma_u^-$	6.85	6.76	6.76	6.73	6.65	6.75[15]
$1^3\Delta_g$	7.27	7.15	7.17	7.14		
$2^1\Sigma_g^+$	7.28	7.32	7.20	7.12		
$2^3\Sigma_g^+$	7.27	7.28	7.21	7.21		
$1^1\Delta_g$	7.37	7.32	7.26	7.20		
$1^1\Sigma_g^-$	7.39	7.31	7.29	7.29		
$1^3\Sigma_g^-$	7.45	7.34	7.36	7.33		
⋮	⋮	⋮	⋮	⋮		
$2^1\Sigma_u^+$	8.13 (2.234 83)	8.07 (2.383 13)	8.03 (2.252 80)	8.05 (2.427 71)	7.81 (0.006 56)	

[a]Spin–free.

The best estimate, obtained at the CCSD(T)/CBS(TQ) +CV(+SO+SR) level, gives the result of $R_{HgBr} = 2.3770$ Å.[21] Without extrapolating to complete basis set limit (CBS) and without accounting for SOC effects for the ground–state structure, and using the aug–cc–pVQZ–PP basis set, the authors obtained an equilibrium geometry of $R_{HgBr} = 2.3897$ Å. Likewise, the geometry optimization of the ground state of this molecule performed in this work at the CASPT2(12,12) level with the distinct basis sets also leads to a linear structure. As can be seen in Table IV, the values obtained with the Def2QZVP, ANO–RCC-VQZP, and Sapp–DKH3–QZP basis sets are closer to the experimental datum, with a difference of around 0.01 Å, whereas the other basis set deviates slightly more, with a difference of 0.036 Å.

The computations of VEEs and *f*, as for IBr, were performed at the MS–CASPT2(IPEA 0.25 a.u.) optimized geometry of the ground state, which belongs to the $D_{\infty h}$ symmetry point group in $HgBr_2$. In order to cover all the energy range of the experimental spectrum, we computed 8 singlet and 8 triplet electronic states for each irrep of the lower symmetry point group D_{2h}: A_g, B_{3u}, B_{2u}, B_{1g}, B_{1u}, B_{2g}, B_{3g}, and A_u. Despite the dipole–forbidden character in the electric dipole approximation of the transition from the X $1\Sigma_g^+$ state, the *gerade* states were also taken into account. The reason is, first, that these states are accessible in electron–collision experiments[56] and, second, that they might be relevant in the photochemistry of $HgBr_2$ since according to the findings obtained by Wadt,[22] the lowest singlet and the lowest triplet states have *gerade* symmetry at the Franck–Condon geometry.

In the previous theoretical work,[22] Wadt ascribed the first band appearing at 5.3–5.4 eV to the $1^1\Sigma_g^+ \rightarrow 1^1\Pi_u$ transition and a more intense band at 6.3–6.4 eV to the $1^1\Sigma_g^+ \rightarrow 1^1\Sigma_u^+$ one. The corresponding transitions computed in the present work are in qualitative agreement with those obtained by Wadt, even though higher VEE values were obtained with the MS–CASPT2 method which are much closer to the experimental data. As can be seen in Table IV, the underestimation of the VEEs is a common feature of the POL(1) CI results for almost all the transitions. Neglecting spin–orbit effects, Wadt assigned the third experimental band at 6.75 eV to the $1^1\Sigma_g^+ \rightarrow 2^1\Sigma_u^+$ transition, even though the computed VEE (7.81 eV) was much higher than the experimental band maximum.[22] This is in contradiction to the results obtained with the current more modern methodology based on the MS–CASPT2 method. Thus, for all the basis sets, MS–CASPT2 predicts this transition to be at ≈8.1 eV with a large value of the corresponding *f*. Moreover, the experimental spectrum of Roxlo and Mandl shows that the band appearing at 6.75 eV is much less intense than the main one at 6.26 eV.[15] As shall be seen below, the computation of the SO states must be carried out for a correct assignment of this band.

Taking into account the more recent experimental spectra,[15] the theoretical values for the low–energy band differ the most for ANO–RCC–VQZP by 0.20 eV, whereas the largest deviation for the band at 6.3 eV is 0.18 eV and corresponds to the Def2QZVP basis set. Regarding the *f*, the Def2QZVP, ANO–RCC–VQZP, and Sapp–DKH3–QZP basis sets show similar agreements with the experiments, namely, a low–energy band is significantly weaker than the other.[15]

On the other hand, the aug–cc–pVQZ–PP basis set predicts similar intensities for the two bands.

To improve the description of the excited states of $HgBr_2$, the SOC is now taken into account. As stated in Secs. I–III, this type of interaction is often relevant for excited states of molecules with heavy atoms. Table V compiles the results obtained for the transitions between the SO states after computing the SOC. One can easily notice that the high–intensity transition computed at 6.3–6.4 eV with the distinct basis sets does not change as compared to the description based on the SF electronic states due to the fact that the $1^1\Sigma_{u\,0+}^+$ excited state maintains its pure singlet nature. On the contrary, the lowest–energy band computed at 5.4–5.5 eV on the basis of the SF states is affected by the SOC effects. Several mixed SO states appear in this region contributing to the experimental band at 5.54[15]/5.39[14] eV. In this case, the performance of the distinct basis sets shows more disagreement as compared to the description of the higher band or the description obtained without considering the SOC. Taking into account only the significant transitions with *f* values of the same order, the Def2QZVP basis set gives rise to three transitions at 5.32, 5.34, and 5.65 eV, the aug–cc–pVQZ–PP basis set has one at 5.49 eV, the ANO–RCC–VQZP has three at 5.33, 5.34, and 5.60 eV, and the Sapp–DKH3–QZP basis set presents three at 5.37, 5.36, and 5.62 eV. These transitions seem to contribute to the experimental band with a band maximum at 5.54[15]/5.39[14] eV. Unfortunately, the dual nature of this band is not evident in the experimental spectrum. Only the aug–cc–pVQZ–PP basis set describes it as a pure singlet transition. However, the predicted *f* value is similar to that of the band at 6.3 eV in contrast to the experiments and the other theoretical data. Regarding the high–energy experimental band at 6.75 eV, which was missing in the description based on the SF states and was ascribed by Wadt to the high $2^1\Sigma_{u\,0+}^+$ state,[22] it can be interpreted now (on the basis of the SO states computed with the Def2QZVP, ANO–RCC–VQZP, and Sapp–DKH3–QZP basis sets) as originated by a transition to the $1^3\Sigma_{u\,0+}^-$ state. This SO state is formed mainly from the $1^3\Sigma_u^-$ state with a small contribution of the $1^1\Sigma_u^+$ SF state, which increases the associated *f*. The results obtained with the aug–cc–pVDZ basis set do not show a significant *f*, which indicates a deficiency of this basis set based on ECPs.

Taking into account the overall information (energies, *f*, and geometries), we conclude that the ANO–RCC–VQZP is an accurate enough basis set for the interpretation of the experimental measurements, with relatively low deviations with respect to the experimental band maxima. The inherent flexibility of the ANO basis sets, as a consequence of the general contraction scheme, may be the reason for its good performance as compared to that of the Sapporo basis set. The latter has more primitive functions, and therefore is more demanding from a computational viewpoint. Hence, in the following we shall focus on the ANO–RCC–VQZP to test the parameters of the multiconfigurational CASSCF/CASPT2 methodology.

In order to verify the minor role of other unoccupied MOs mainly originated from linear combinations of 6*d* and 4*d* AOs of Hg and Br, respectively, we computed the VEEs and corresponding *f* between SO states with a larger active

TABLE V. Main vertical excitation energies (VEEs) in eV and associated oscillator strength (f) values (within parentheses) obtained for $HgBr_2$ from the computation of the SO states with the SOC–MS–CASPT2(12,12)–IPEA(0.25 a.u.) methodology and distinct basis sets. Experimental data included for comparison.

Basis set SO[a] state	Def2QZVP	aug–cc–pVQZ–PP	ANO–RCC–VQZP	Sapp–DKH3–QZP	Expt.
$1\,^3\Pi_{g2}$	4.47	4.63	4.42	4.45	
$1\,^3\Pi_{g1}$	4.54	4.64	4.49	4.52	
$1\,^3\Pi_{g0-}$	4.72	4.66	4.73	4.75	
$1\,^3\Pi_{g0+}$	4.72	4.66	4.73	4.76	
$1\,^1\Pi_{g1}$	4.86	4.90	4.84	4.86	
$1\,^3\Pi_{u2}$	5.12	5.33	5.04	5.06	
$1\,^3\Pi_{u1}$	5.17 (0.002 81)	5.34 (0.000 11)	5.10 (0.006 25)	5.13 (0.004 02)	
$1\,^3\Pi_{u0-}$	5.23	5.35	5.26	5.29	
$1\,^1\Pi_{u1}$	5.32 (0.015 33)	5.49 (0.030 31)	5.33 (0.014 15)	5.37 (0.011 14)	5.54,[15] 5.39[14]
$1\,^3\Pi_{u0+}$	5.34 (0.009 68)	5.35 (0.000 05)	5.34 (0.007 59)	5.36 (0.007 04)	
$1\,^3\Sigma^+_{u0-}$	5.61	5.61	5.56	5.58	
$1\,^3\Sigma^+_{u1}$	5.65 (0.009 00)	5.61 (0.000 18)	5.60 (0.008 54)	5.62 (0.006 89)	
$2\,^3\Sigma^+_{u1}$	6.50 (0.000 09)	6.47 (0.000 00)	6.23 (0.000 02)	6.24 (0.000 02)	
$1\,^3\Delta_{u2}$	6.56	6.60	6.27	6.27	
$1\,^1\Sigma^+_{u0+}$	6.43 (0.085 75)	6.37 (0.059 17)	6.37 (0.109 46)	6.37 (0.087 25)	6.26,[15] 6.36[14]
$2\,^3\Sigma^+_{u0-}$	6.51	6.47	6.48	6.49	
$1\,^3\Delta_{u1}$	6.80 (0.000 87)	6.61 (0.000 00)	6.55 (0.000 37)	6.54 (0.000 43)	
$1\,^3\Sigma^+_{g1}$	6.77	6.78	6.64	6.61	
$1\,^3\Delta_{u3}$	6.59	6.59	6.71	6.72	
$1\,^3\Sigma^+_{g0-}$	6.78	6.78	6.73	6.70	
$1\,^1\Sigma^-_{u0-}$	6.81	6.62	6.74	6.72	
$1\,^3\Sigma^-_{u0+}$	6.86 (0.015 04)	6.76 (0.000 07)	6.79 (0.004 30)	6.77 (0.007 30)	6.75[15]
$1\,^3\Delta_{g2}$	7.18	7.15	6.86	6.80	
$1\,^1\Delta_{u2}$	6.83	6.55	6.99	6.98	
$1\,^3\Sigma^-_{u1}$	6.90 (0.000 69)	6.76 (0.000 00)	7.05 (0.000 72)	7.04 (0.000 81)	
$2\,^3\Sigma^+_{g1}$	7.24	7.28	7.06	7.04	
$1\,^3\Delta_{g1}$	7.32	7.17	7.10	7.08	
$2\,^3\Sigma^+_{g0-}$	7.24	7.28	7.18	7.18	
$2\,^1\Sigma^+_{g0+}$	7.26	7.32	7.19	7.12	
$1\,^3\Delta_{g3}$	7.17	7.15	7.26	7.25	
$1\,^1\Sigma^-_{g0-}$	7.39	7.31	7.33	7.34	
$1\,^3\Sigma^-_{g0+}$	7.44	7.35	7.38	7.36	
$1\,^1\Delta_{g2}$	7.40	7.26	7.56	7.56	
$1\,^3\Sigma^-_{g1}$	7.46	7.35	7.61	7.60	
⋮	⋮	⋮	⋮	⋮	⋮
$2\,^1\Sigma^+_{u0+}$	8.13 (2.209 64)	8.07 (2.383 07)	8.06 (2.196 53)	8.08 (2.235 95)	

[a]Spin–free.

space, CAS(22,15), as mentioned above in Sec. II. The results show negligible differences in geometry, energies, and f values (see Table S.VI, supplementary material). Most importantly, the description of all states is similar, thus confirming that the band at 6.75 eV has $1\,^3\Sigma^-_{u0+}$ character, as opposed to the $2\,^1\Sigma^+_{u0+}$ nature proposed by Wadt on the basis of POL(1) CI calculations without accounting for the SOC. We also conclude that the CAS(12,12) configurational space is accurate for the description of the absorption spectrum and that no excitations of electrons from the $5d$ subshell occur. This fact may be an important observation for further studies of other mercury–halogen compounds, such as $HgCl_2$ and HgBrOBr, in which mercury forms strictly covalent bonds.

Next, to discard any effect due to the mixing of high–energy CASSCF wavefunctions in the immediately lower states, we tested the stability of the results upon changing the number of averaged roots. Five, eight, and eleven roots for each set of irreps were considered, obtaining the results compiled in Table S.VII of the supplementary material. It follows that the energy values are very similar, in particular those obtained with 8 and 11 roots, with deviations lower than 0.08 eV. Absolute f values are more sensitive. Nevertheless, the relative intensity of the transitions is still maintained on the same level.

Regarding the analysis of the effect of the IPEA shift in the MS–CASPT2 computations, Table S.VIII (supplementary material) compiles the results without shift and with the recommended value of 0.25 a.u. As for IBr, one can see again a systematic underestimation of the transition energies, in this case, with energy differences of around 0.3–0.4 eV. Thus, the 0.25 a.u. IPEA shift shall be used for accurate determinations of the absorption spectra with the presently calibrated methodology.

TABLE VI. Vertical excitation energies (VEEs) in eV and associated oscillator strength (f) values (within parentheses) of $HgBr_2$ computed at the CASPT2(12,12)–IPEA(0.25 a.u.)/ANO–RCC–VQZP level with the SS and MS approaches and on the basis of both the SF and SO states. Experimental data included for comparison.

SF[a] state	Without spin–orbit coupling		SO[b] state		With spin–orbit coupling		
	SS–CASPT2	MS–CASPT2			SS–CASPT2	MS–CASPT2	Expt.
$1^3\Pi_u$	5.16	5.17	$(1)1_u$	$(1^3\Pi_{u1})$	5.10 (0.008 06)	5.10 (0.006 25)	
			$(1)0_u^+$	$(1^3\Pi_{u0+})$	5.33 (0.006 08)	5.34 (0.007 59)	
$1^1\Pi_u$	5.37 (0.045 17)	5.34 (0.029 03)	$(2)1_u$	$(1^1\Pi_{u1})$	5.36 (0.020 78)	5.33 (0.014 15)	5.54,[15] 5.39[14]
$1^3\Sigma_u^+$	5.47	5.46	$(3)1_u$	$(1^3\Sigma_{u1}^+)$	5.59 (0.016 06)	5.60 (0.008 54)	
$2^3\Sigma_u^+$	6.40	6.47	$(4)1_u$	$(2^3\Sigma_{u1}^+)$	6.20 (0.000 08)	6.23 (0.000 02)	
$1^1\Sigma_u^+$	6.39 (0.001 38)	6.35 (0.116 13)	$(2)0_u^+$	$(1^1\Sigma_{u0+}^+)$	6.39 (0.000 93)	6.37 (0.109 46)	6.26,[15] 6.36[14]
$1^3\Delta_u$	6.57	6.61	$(5)1_u$	$(1^3\Delta_{u1})$	6.52 (0.000 51)	6.55 (0.000 37)	
$1^3\Sigma_u^-$	6.73	6.76	$(3)0_u^+$	$(1^3\Sigma_{u0+}^-)$	6.76 (0.000 57)	6.79 (0.004 30)	6.75[15]
			$(6)1_u$	$(1^3\Sigma_{u1}^-)$	7.00 (0.000 56)	7.05 (0.000 72)	
$2^1\Sigma_u^+$	8.06 (2.273 43)	8.03 (2.252 80)	$(4)0_u^+$	$(2^1\Sigma_{u0+}^+)$	8.09 (2.198 53)	8.06 (2.196 53)	

[a]Spin–free.
[b]Spin–orbit.

Finally, the comparison of the results obtained with the SS– and MS–CASPT2 methods shows a good agreement of the VEEs (see Table VI). In contrast, a significant discrepancy occurs for the f values of the band at 6.39-6.35 eV. The SS method predicts a very weak band in contrast to the MS result and the experimental data. We try to provide here an explanation for this finding. For this SF state ($1^1\Sigma_u^+$), one can observe a non negligible mixing with a higher state with the same symmetry, $2^1\Sigma_u^+$, described mainly with the electronic configuration $\sigma_g^{+2} \pi_u^{nb4} \pi_{g,p}^{nb4} \sigma_u^{+nb1} \sigma_g^{+*1} \pi_u^0$ (see Table VII). Thus, after diagonalization of the symmetrized effective Hamiltonian matrix, the new eigenvector of $1^1\Sigma_u^+$ is formed as a slight mixture of both SS–CASPT2 states, with the weights of 0.982^2 and 0.175^2, respectively. This does not have a big impact on the VEEs, as shown in Table VI. However, the fact that the singlet–singlet transition to $2^1\Sigma_u^+$ (obtained at the SS–CASPT2 level) is extremely intense (VEE = 8.03 eV, f = 2.252 80) might produce a great increase of the f value and hence the probability of the transition. In the MS–CASPT2 method, the TDM is computed with the first–order corrected wavefunctions, while the SS method uses the CASSCF wavefunction. This phenomenon is not observed for other states in this molecule, neither in IBr. The improved wavefunction used in the MS might be needed for an accurate description of the f values.

In general, the MS-CASPT2(12,12)/ANO–RCC–VQZP method accounting for the SOC with 8 averaged roots in each symmetry and with the recommended value of 0.25 a.u. for the IPEA shift allows a good prediction of the absorption properties of the molecule as compared to the experimental spectrum (see Fig. 4).

Taking into account the electronic structure analysis of the SF states (see electronic configurations in Table VII) and SO states (see contribution of the SF states in Table VIII), the intense band appearing at ≈6.3 eV can be assigned to an electronic transition between singlet states, $1^1\Sigma_g^+ \rightarrow 1^1\Sigma_u^+$, which mainly corresponds to the transfer of electron density from the Br atoms to Hg. As can be seen in Table VII, two configurations are mainly involved in the transition to the $1^1\Sigma_u^+$ state. The most relevant one (with a weight of 65%) corresponds to

an electron excitation from the $\pi_{g,p}^{nb}$ orbital localized in the Br atoms to the π_u orbital of Hg. Meanwhile, the other electronic configuration (with a weight of 25%) involves the excitation from the σ_u^{+nb} non–bonding orbital of the Hg–Br bonds to the corresponding anti–bonding orbital, σ_g^{+*}. The $2^1\Sigma_u^+$ state is also characterized by the contribution of such configurations, even though in this case the weights are inverted

TABLE VII. Main electronic configurations of the most relevant *ungerade* low–lying electronic states in the UV-Vis spectroscopy of $HgBr_2$ determined with the CASSCF(12,12)/ANO–RCC–VQZP methodology at the MS–CASPT2 optimized geometry (R_{HgBr} = 2.363 Å). For *gerade* states, see Table S.IX, supplementary material.

| SF[a] state	Configuration	Weight (%)
$1^1\Sigma_g^+$	$\sigma_g^{+2} \pi_u^{nb4} \pi_{g,p}^{nb4} \sigma_u^{+nb2} \sigma_g^{+*0} \pi_u^0$	95
$1^1\Sigma_u^+$	$\sigma_g^{+2} \pi_u^{nb4} \pi_{g,p}^{nb3} \sigma_u^{+nb2} \sigma_g^{+*0} \pi_u^1$	65
	$\sigma_g^{+2} \pi_u^{nb4} \pi_{g,p}^{nb4} \sigma_u^{+nb1} \sigma_g^{+*1} \pi_u^0$	25
	$\sigma_g^{+2} \pi_u^{nb3} \pi_{g,p}^{nb4} \sigma_u^{+nb1} \sigma_g^{+*1} \pi_u^1$	3
$2^1\Sigma_u^+$	$\sigma_g^{+2} \pi_u^{nb4} \pi_{g,p}^{nb4} \sigma_u^{+nb1} \sigma_g^{+*1} \pi_u^0$	61
	$\sigma_g^{+2} \pi_u^{nb4} \pi_{g,p}^{nb3} \sigma_u^{+nb2} \sigma_g^{+*0} \pi_u^1$	24
	$\sigma_g^{+2} \pi_u^{nb3} \pi_{g,p}^{nb4} \sigma_u^{+nb2} \sigma_g^{+*0} \pi_u^0 \pi_g^1$	8
$1^1\Pi_u$	$\sigma_g^{+2} \pi_u^{nb3} \pi_{g,p}^{nb4} \sigma_u^{+nb2} \sigma_g^{+*1} \pi_u^0$	87
	$\sigma_g^{+2} \pi_u^{nb4} \pi_{g,p}^{nb3} \sigma_u^{+nb1} \sigma_g^{+*2} \pi_u^0$	5
	$\sigma_g^{+2} \pi_u^{nb4} \pi_{g,p}^{nb3} \sigma_u^{+nb2} \sigma_g^{+*0} \pi_u^0 \sigma_u^{+1}$	3
$1^1\Sigma_u^-$	$\sigma_g^{+2} \pi_u^{nb4} \pi_{g,p}^{nb3} \sigma_u^{+nb2} \sigma_g^{+*0} \pi_u^1$	89
	$\sigma_g^{+2} \pi_u^{nb3} \pi_{g,p}^{nb4} \sigma_u^{+nb1} \sigma_g^{+*1} \pi_u^1$	4
$1^1\Delta_u$	$\sigma_g^{+2} \pi_u^{nb4} \pi_{g,p}^{nb3} \sigma_u^{+nb2} \sigma_g^{+*0} \pi_u^1$	89
	$\sigma_g^{+2} \pi_u^{nb3} \pi_{g,p}^{nb4} \sigma_u^{+nb1} \sigma_g^{+*1} \pi_u^1$	4
$1^3\Sigma_u^+$	$\sigma_g^{+2} \pi_u^{nb4} \pi_{g,p}^{nb4} \sigma_u^{+nb1} \sigma_g^{+*1} \pi_u^0$	87
	$\sigma_g^{+2} \pi_u^{nb4} \pi_{g,p}^{nb3} \sigma_u^{+nb2} \sigma_g^{+*0} \pi_u^1$	6
$2^3\Sigma_u^+$	$\sigma_g^{+2} \pi_u^{nb4} \pi_{g,p}^{nb3} \sigma_u^{+nb2} \sigma_g^{+*0} \pi_u^1$	83
	$\sigma_g^{+2} \pi_u^{nb4} \pi_{g,p}^{nb4} \sigma_u^{+nb1} \sigma_g^{+*1} \pi_u^0$	6
	$\sigma_g^{+2} \pi_u^{nb3} \pi_{g,p}^{nb4} \sigma_u^{+nb1} \sigma_g^{+*1} \pi_u^1$	4
$1^3\Pi_u$	$\sigma_g^{+2} \pi_u^{nb3} \pi_{g,p}^{nb4} \sigma_u^{+nb2} \sigma_g^{+*1} \pi_u^0$	88
	$\sigma_g^{+2} \pi_u^{nb4} \pi_{g,p}^{nb3} \sigma_u^{+nb1} \sigma_g^{+*2} \pi_u^0$	3
$1^3\Sigma_u^-$	$\sigma_g^{+2} \pi_u^{nb4} \pi_{g,p}^{nb3} \sigma_u^{+nb2} \sigma_g^{+*0} \pi_u^1$	90
	$\sigma_g^{+2} \pi_u^{nb3} \pi_{g,p}^{nb4} \sigma_u^{+nb1} \sigma_g^{+*1} \pi_u^1$	4
$1^3\Delta_u$	$\sigma_g^{+2} \pi_u^{nb4} \pi_{g,p}^{nb3} \sigma_u^{+nb2} \sigma_g^{+*0} \pi_u^1$	89
	$\sigma_g^{+2} \pi_u^{nb3} \pi_{g,p}^{nb4} \sigma_u^{+nb1} \sigma_g^{+*1} \pi_u^1$	4

[a]Spin–free.
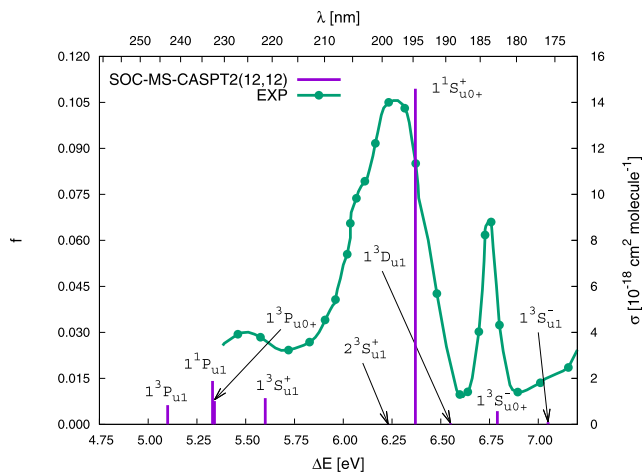
FIG. 4. Graphical representation of the vertical excitation energies (VEEs) in eV (ΔE) and nm (λ) and associated f for the SO states of $HgBr_2$ computed at the MS–CASPT2(12,12)–IPEA(0.25 a.u.)/ANO–RCC–VQZP level (purple, sticks), and the experimental absorption cross sections σ (dark green line, circles).[15]

(see Table VII). This multiconfigurational character of the $1^1\Sigma_u^+$ and $2^1\Sigma_u^+$ states was already predicted by Wadt on the basis of the POL(1) CI wave function analysis.[22] However, the dominant configurations in the two states were found to be the opposite as those obtained in the present work. Note that the computations by Wadt were carried out at the experimental value for the Hg–Br bond length (2.410 Å), whereas the VEEs were computed in this work at the MS–CASPT2 ground–state optimized geometry (2.363 Å). To search for an explanation of the mentioned discrepancy, we analyzed the CASSCF wave functions and the MS–CASPT2 state mixing along the stretching mode of the Hg–Br bonds with the constraint

TABLE VIII. Main contributions of the pure SF states to the mixed SO states of $HgBr_2$. Values correspond to the MS–CASPT2(12,12)–IPEA(0.25 a.u.)/ANO-RCC-QVZP computations.

	SO[a] state	Weight (%)	SF[b] state	ΔE (eV) (Osc.)
(1)1_u	($1^3\Pi_{u1}$)	77	$1^3\Pi_u$	5.10 (0.006 25)
		22	$1^1\Pi_u$	
(2)0_u^+	($1^3\Pi_{u0+}$)	100	$1^3\Pi_u$	5.34 (0.007 59)
(2)1_u	($1^1\Pi_{u1}$)	49	$1^1\Pi_u$	5.33 (0.014 15)
		41	$1^3\Sigma_u^+$	
		10	$1^3\Pi_u$	
(3)1_u	($1^3\Sigma_{u\,1}^+$)	58	$1^3\Sigma_u^+$	5.60 (0.008 54)
		29	$1^1\Pi_u$	
		13	$1^3\Pi_u$	
(4)1_u	($2^3\Sigma_{u\,1}^+$)	68	$2^3\Sigma_u^+$	6.23 (0.000 02)
		32	$1^3\Sigma_u^-$	
(3)0_u^+	($1^1\Sigma_{u\,0+}^+$)	99	$1^1\Sigma_u^+$	6.37 (0.109 46)
		1	$1^3\Sigma_u^-$	
(5)1_u	($1^3\Delta_{u1}$)	100	$1^3\Delta_u$	6.55 (0.000 37)
(4)0_u^-	($1^3\Sigma_{u\,0+}^-$)	99	$1^3\Sigma_u^-$	6.79 (0.004 30)
		1	$1^1\Sigma_u^+$	
(6)1_u	($1^3\Sigma_{u\,1}^-$)	68	$1^3\Sigma_u^-$	7.05 (0.000 72)
		32	$2^3\Sigma_u^+$	
(5)0_u^+	($2^1\Sigma_{u\,0+}^+$)	99	$2^1\Sigma_u^+$	8.06 (2.196 53)
		1	$2^3\Pi_u$	

[a]Spin–orbit.
[b]Spin–free.

of D_{2h} symmetry and focusing on the contributions of the $\pi_{g,p}^{nb} \rightarrow \pi_u$ and $\sigma_u^{+nb} \rightarrow \sigma_g^{+*}$ configurations in the $1^1\Sigma_u^+$ and $2^1\Sigma_u^+$ states (Table S.X, supplementary material). Similarly, the effect of the bending mode was also determined for the low–energy state originating from $1^1\Sigma_u^+$–$^1B_2$, with the C_{2v} symmetry constraint (see Table S.XI and natural orbitals in Fig. S.1, supplementary material). The relative contributions of the two relevant electronic configurations do not change significantly in the CASSCF wave function along the bond stretching. However, the $1^1\Sigma_u^+$ and $2^1\Sigma_u^+$ states show a strong mixing in the eigenvectors of the effective Hamiltonian matrix of the MS–CASPT2 procedure, and they are more sensitive to the bond distance. The resulting mixed state configurations show a change in the trend along the bond length coordinate. Thus, at short R_{HgBr} values, the $\pi_{g,p}^{nb} \rightarrow \pi_u$ configuration has a larger weight in the $1^1\Sigma_u^+$ state than the $\sigma_u^{+nb} \rightarrow \sigma_g^{+*}$ configuration. As the bond stretches, the lower–energy state gains more $\sigma_u^{+nb} \rightarrow \sigma_g^{+*}$ character. This finding may be qualitatively explained taking into account the correlations between the MOs of the molecule and the AOs of the dissociated atoms. The $\pi_{g,p}^{nb}$ and σ_u^{+nb} MOs correlate with the $4p_{x,y,z}$ AOs of Br, which have the same energy (see Fig. 2). Meanwhile, the σ_g^{+*} and π_u correlate with the 6s and $6p_{x,y}$ of Hg, respectively, and the latter is more energetic. The energy gap between the $4p_{x,y,z}$ Br and 6s Hg AOs is lower than the energy difference between the $4p_{x,y,z}$ Br and $6p_{x,y}$ Hg AOs. Consequently, the gap between the σ_u^{+nb} and σ_g^{+*} MOs upon increasing R_{HgBr} is lower than the energy difference between the $\pi_{g,p}^{nb}$ and π_u MOs. Regarding the bending mode effect, the non–linear geometries magnify the $22b_2 \rightarrow 31a_1$ nature of the $^1B_2$ state (which corresponds to the $\sigma_u^{+nb} \rightarrow \sigma_g^{+*}$ character of the $1^1\Sigma_u^+$ state for the linear structure) (see Table S.XI, supplementary material).

In general, the $1^1\Sigma_u^+$ state, which is ascribed to the highest–intensity band in the experimental spectrum of Figure 4, is characterized by a partial population of the σ_g^{+*} orbital. This explains the larger bond length obtained at the equilibrium structure of the $1^1\Sigma_u^+$ state as compared to that of the ground state (see Table IX). In addition, the geometry becomes bent with an angle of 84.7°. The finding supports previous estimations of the excited–state geometry based on the mapping of the PECs at different bending angles.[22] Analogous PECs were also computed in the present work for the sake of comparison (see Fig. S.2, supplementary material).

In contrast to the band at ≈6.3 eV with a singlet–singlet nature, the low–energy experimental band with a maximum at 5.54[15]/5.39[14] eV is produced by electronic transitions with strong SOC. For example, the SO states (2)1 and (3)1 have almost equal contributions of the singlet $1^1\Pi$ and triplet $1^3\Sigma_u^+$ SF states. As can be seen in Table VII and in Fig. 2, the electron promotion takes place now mainly from the non–bonding p–type atomic orbitals (π_u^{nb}) of the Br atoms and the σ_u^{+nb} of the Hg–Br bonds to the anti–bonding σ_g^{+*} orbital. The change of the electronic structure from the ground state to the $1^1\Pi_u$ and $1^3\Sigma_u^+$ SF states, which are related to the weak band of the spectrum, implies a large increase of the bond length of 0.4–0.5 Å to reach the equilibrium structure of such excited states (see Table IX). The bond angle decreases to 115.4/109.3 and 83.3° for the $1^1\Pi_u$ and $1^3\Sigma_u^+$ SF states (which

TABLE IX. Equilibrium geometries of relevant low–lying SF states of HgBr$_2$ (with the constraint of C$_{2v}$ symmetry). The MS–CASPT2/ANO-RCC-VQZP methodology was used here with a smaller active space (12,10) and 5 roots. Structures are demonstrated to be minima by means of the computations of the frequencies with the constraint of C$_s$ symmetry (see Table S.XII, supplementary material). Main electronic configurations and their weights are also included (see corresponding natural orbitals in Fig. S.1, supplementary material).

$D_{\infty h}$[a]	C_{2v}	R_{HgBr} (Å)	$\angle_{BrHgBr}$ (deg)	Mixed state configuration[b]	Weight (%)
$1^1\Sigma_g^+$	$^1A_1$	2.363	180.0	$29a_1^2\ 30a_1^2\ 31a_1^0\ 32a_1^0\ 14b_1^2\ 15b_1^0\ 21b_2^2\ 22b_2^2\ 23b_2^0\ 9a_2^2$	96
$1^1\Pi_u$	$^1A_1$	2.848	115.4	$29a_1^1\ 30a_1^2\ 31a_1^1\ 32a_1^0\ 14b_1^2\ 15b_1^0\ 21b_2^2\ 22b_2^2\ 23b_2^0\ 9a_2^2$	72
				$29a_1^2\ 30a_1^2\ 31a_1^2\ 32a_1^0\ 14b_1^2\ 15b_1^0\ 21b_2^2\ 22b_2^0\ 23b_2^0\ 9a_2^2$	10
				$29a_1^2\ 30a_1^2\ 31a_1^2\ 32a_1^0\ 14b_1^2\ 15b_1^0\ 21b_2^0\ 22b_2^2\ 23b_2^0\ 9a_2^2$	7
	$^1B_1$	2.848	109.3	$29a_1^2\ 30a_1^2\ 31a_1^1\ 32a_1^0\ 14b_1^1\ 15b_1^0\ 21b_2^2\ 22b_2^2\ 23b_2^0\ 9a_2^2$	74
				$29a_1^2\ 30a_1^2\ 31a_1^2\ 32a_1^0\ 14b_1^2\ 15b_1^0\ 21b_2^2\ 22b_2^1\ 23b_2^0\ 9a_2^1$	17
$1^1\Sigma_u^+$	$^1B_2$	2.649	84.7	$29a_1^2\ 30a_1^2\ 31a_1^1\ 32a_1^0\ 14b_1^2\ 15b_1^0\ 21b_2^2\ 22b_2^1\ 23b_2^0\ 9a_2^2$	82
				$29a_1^2\ 30a_1^2\ 31a_1^1\ 32a_1^0\ 14b_1^2\ 15b_1^0\ 21b_2^1\ 22b_2^2\ 23b_2^0\ 9a_2^2$	6
$2^1\Sigma_u^+$	$^1B_2$	2.521	178.8	$29a_1^2\ 30a_1^2\ 31a_1^0\ 32a_1^1\ 14b_1^2\ 15b_1^0\ 21b_2^1\ 22b_2^2\ 23b_2^0\ 9a_2^2$	32
				$29a_1^2\ 30a_1^2\ 31a_1^0\ 32a_1^0\ 14b_1^2\ 15b_1^1\ 21b_2^2\ 22b_2^2\ 23b_2^0\ 9a_2^1$	31
				$29a_1^2\ 30a_1^2\ 31a_1^1\ 32a_1^0\ 14b_1^2\ 15b_1^0\ 21b_2^2\ 22b_2^1\ 23b_2^0\ 9a_2^2$	27
$1^3\Pi_u$	$^3A_1$	2.755	123.5	$29a_1^1\ 30a_1^2\ 31a_1^1\ 32a_1^0\ 14b_1^2\ 15b_1^0\ 21b_2^2\ 22b_2^2\ 23b_2^0\ 9a_2^2$	80
				$29a_1^2\ 30a_1^2\ 31a_1^2\ 32a_1^0\ 14b_1^2\ 15b_1^0\ 21b_2^2\ 22b_2^1\ 23b_2^0\ 9a_2^2$	10
	$^3B_1$	2.803	132.9	$29a_1^2\ 30a_1^2\ 31a_1^1\ 32a_1^0\ 14b_1^1\ 15b_1^0\ 21b_2^2\ 22b_2^2\ 23b_2^0\ 9a_2^2$	78
				$29a_1^2\ 30a_1^2\ 31a_1^2\ 32a_1^0\ 14b_1^2\ 15b_1^0\ 21b_2^1\ 22b_2^2\ 23b_2^0\ 9a_2^1$	12
$1^3\Sigma_u^+$	$^3B_2$	2.766	83.3	$29a_1^2\ 30a_1^2\ 31a_1^1\ 32a_1^0\ 14b_1^2\ 15b_1^0\ 21b_2^2\ 22b_2^1\ 23b_2^0\ 9a_2^2$	46
				$29a_1^2\ 30a_1^2\ 31a_1^1\ 32a_1^0\ 14b_1^2\ 15b_1^0\ 21b_2^1\ 22b_2^2\ 23b_2^0\ 9a_2^2$	39
$1^3\Sigma_u^-$	$^3A_2$	2.392	180.0	$29a_1^2\ 30a_1^2\ 31a_1^0\ 32a_1^1\ 14b_1^2\ 15b_1^0\ 21b_2^2\ 22b_2^2\ 23b_2^0\ 9a_2^1$	43
				$29a_1^2\ 30a_1^2\ 31a_1^0\ 32a_1^0\ 14b_1^2\ 15b_1^1\ 21b_2^2\ 22b_2^1\ 23b_2^0\ 9a_2^2$	47

[a]Spin–free state.

[b]Obtained at MS–CASPT2 level of theory.

become $^1A_1$/$^1B_1$ and $^3B_2$ states in C$_{2v}$ symmetry, respectively). This is in agreement with the estimations obtained by Wadt.[22] The geometrical parameters of the equilibrium structure of the $1^3\Pi_u$ state are similar to those found for the $1^1\Pi_u$ state (see Table IX). The former mainly gives rise to the $1^3\Pi_{u1}$ and $1^3\Pi_{u0+}$ SO states which also contribute to the experimental spectrum.

Regarding the band at 6.75 eV, it is ascribed in this work to the $1^3\Sigma_{u0+}^-$ state, whose transition is basically described by a $\pi_{g,p}^{nb} \to \pi_u$ excitation (see Table VII). Due to the fact that the electron density redistribution does not imply a significant occupation of anti–bonding orbitals in the electronic transition, the state keeps an equilibrium structure very close to that of the ground state. Thus, R$_{HgBr}$ only increases by 0.03 Å and the molecule is maintained linear. This is in agreement with the shape of the experimental band with a very small energy difference between the band maximum and the band origin. Similar to $1^3\Sigma_{u0+}^-$, the $2^1\Sigma_{u0+}^+$ state, which is ascribed in this work to the high–energy band at around 8 eV (not shown in the experimental spectrum), is dominated by the $\pi_{g,p}^{nb} \to \pi_u$ excitation, with partial occupation of the σ_g^{+*} orbital. Accordingly, the optimized geometry for this state maintains the linearity and has a lower bond stretching than that found for other states with a large occupation of anti–bonding orbitals, such as the $1^1\Sigma_{u0+}^+$ state.

IV. SUMMARY AND CONCLUSIONS

The CASSCF/MS–CASPT2/SO–RASSI quantum-chemical methodology has been used in the present study to determine the absorption properties of two representative mercury/halogen compounds in atmospheric chemistry, IBr and HgBr$_2$. An in-depth comparison with previous theoretical results obtained with distinct methodologies[9,10] and data recorded in experiments[3,14,15] has allowed us to calibrate several aspects of the employed multireference methods. Among the four basis sets used, Def2QZVP, aug–cc–pVQZ–PP, ANO–RCC–VQZP, and Sapporo–DKH3–QZP, those with effective–core potentials (the first two) have provided poor descriptions in some cases with strong spin–orbit couplings (SOC), and therefore they are not adequate for an accurate and general determination of electronic transitions in systems similar to those studied here. The ANO–RCC basis set has shown to be particularly efficient due to its general contraction scheme, which makes it more flexible in the characterization of the excited states. Meanwhile, the IPEA shift of 0.25 a.u. of the CASPT2 method has improved the transition energies by 0.2–0.4 eV with respect to the results obtained with the non–modified zeroth–order Hamiltonian of the CASPT2. The single– and multi–state approaches of the CASPT2 have given rise to basically the same energies, although the latter has provided a better description of the relative intensity of the absorption bands in HgBr$_2$. Finally, our calibration shows that a description based on the spin–orbit (SO) states rather than the spin–free (SF) states is mandatory for these halogen/mercury molecular systems since some bands arise as the result of the SOC.

Besides the calibrations, we have also described the properties of the electronic transitions and the nature of the experimental bands. In the case of IBr, in which high-level theoretical studies have been carried out by Patchkovskii[9] and

Li *et al.*[10] in previous works, the MS–CASPT2 computations have confirmed these early findings. For $HgBr_2$, the first theoretical information on the low–lying excited states and the first interpretation of the experimental spectrum based on the SO states have been presented here. The high–intensity band at 6.26[15]/6.36[14] eV has been found to be a pure singlet–singlet electronic transition, $1\,^1\Sigma^+_{g\,0+} \rightarrow 1\,^1\Sigma^+_{u\,0+}$. The weak and broad band at 5.54[15]/5.39[14] eV has a more complex nature involving several singlet–singlet and singlet–triplet transitions to low–lying Σ and Π SO states. Previous results obtained by Wadt[22] without accounting for the SOC were reproduced and updated with a different description of the band peaking at 6.75 eV, corresponding to a singlet–triplet transition to the $1\,^3\Sigma^-_{u\,0+}$ state rather than a transition to the high–energy $2\,^1\Sigma^+_{u\,0+}$ singlet state.

In general, the MS–CASPT2 method, taking into account the SOC (through RASSI procedure), the IPEA shift with a value of 0.25 a.u., and the ANO–RCC basis set (with the DKH3 Hamiltonian), has shown to be an appropriate methodological approach for a general and accurate enough (±0.1–0.2 eV) determination of the cross sections of atmospheric compounds containing halogen atoms and/or mercury.

SUPPLEMENTARY MATERIAL

See supplementary material for: (1) Tables S.I-V which compile the results of the calibration of the number of SA-CASSCF and MS-CASPT2 roots, the IPEA shift, and SS- vs MS-CASPT2 approaches for IBr along with configurations of excited states of interests, (2) Tables S.V-IX which compile the results of the calibration of the number of orbitals in the CAS, the number of SA-CASSCF and MS-CASPT2 roots, and the IPEA shift for $HgBr_2$, (3) Tables S.X-XI which compile the change of CASSCF configurations of states of interests for chosen distorted geometries, (4) Table S.XII which compiles the vibrational frequencies of excited states optimized with the constraint of C_{2v} symmetry, (5) Figure S.1 which presents the selected active space for calculations in C_{2v} symmetry for bent structures of $HgBr_2$, and (6) Figure S.2 which shows the potential energy curves as a function of the bending angle of $HgBr_2$.

ACKNOWLEDGMENTS

[1]A. Saiz-Lopez and R. von Glasow, Chem. Soc. Rev. **41**, 6448 (2012).

[2]A. Steffen, T. Douglas, M. Amyot, P. Ariya, K. Aspmo, T. Berg, J. Bottenheim, S. Brooks, F. Cobbett, A. Dastoor, A. Dommergue, R. Ebinghaus,

C. Ferrari, K. Gardfeldt, M. E. Goodsite, D. Lean, A. J. Poulain, C. Scherz, H. Skov, J. Sommar, and C. Temme, Atmos. Chem. Phys. **8**, 1445 (2008).

[3]D. J. Seery and D. Britton, J. Phys. Chem. **68**, 2263 (1964).

[4]W. Holzer, W. F. Murphy, and H. J. Bernstein, J. Chem. Phys. **52**, 469 (1970).

[5]T. Yukiya, N. Nishimiya, and M. Suzuki, J. Mol. Spectrosc. **214**, 132 (2002).

[6]W. G. Brown, Phys. Rev. **42**, 355 (1932).

[7]M. Macler, M. Erickson, H.-S. Lin, and M. C. Heaven, J. Phys. Chem. **96**, 4301 (1992).

[8]J. Pittner and P. Jungwirth, Chem. Phys. Lett. **321**, 281 (2000).

[9]S. Patchkovskii, Phys. Chem. Chem. Phys. **8**, 926 (2006).

[10]R. Li, C. Wei, Q. Sun, E. Sun, M. Jin, H. Xu, and B. Yan, J. Quant. Spectrosc. Radiat. Transfer **133**, 271 (2014).

[11]M. E. Goodsite, J. M. C. Plane, and H. Skov, Environ. Sci. Technol. **38**, 1772 (2004).

[12]T. S. Dibble, M. J. Zelie, and H. Mao, Atmos. Chem. Phys. **12**, 10271 (2012).

[13]F. Wang, A. Saiz-Lopez, A. S. Mahajan, J. C. Gómez Martín, D. Armstrong, M. Lemes, T. Hay, and C. Prados-Roman, Atmos. Chem. Phys. **14**, 1323 (2014).

[14]J. Maya, J. Chem. Phys. **67**, 4976 (1977).

[15]C. Roxlo and A. Mandl, J. Appl. Phys. **51**, 2969 (1980).

[16]V. Barone, A. Bencini, F. Totti, and M. G. Uytterhoeven, Int. J. Quantum Chem. **61**, 361 (1995).

[17]P. Schwerdtfeger, P. D. W. Boyd, S. Brienne, J. S. McFeaters, M. Dolg, M. S. Liao, and W. H. Eugen Schwarz, Inorg. Chim. Acta **213**, 233 (1993).

[18]A. F. Khalizov, B. Viswanathan, P. Larregaray, and P. A. Ariya, J. Phys. Chem. A **107**, 6360 (2003).

[19]M. Kaupp and H. G. Von Schnering, Inorg. Chem. **33**, 4179 (1994).

[20]J. Kim, H. Ihee, and Y. S. Lee, J. Chem. Phys. **133**, 144309 (2010).

[21]N. B. Balabanov and K. A. Peterson, J. Chem. Phys. **119**, 12271 (2003).

[22]W. R. Wadt, J. Chem. Phys. **72**, 2469 (1980).

[23]J. Finley, P.-Å. Malmqvist, B. O. Roos, and L. Serrano-Andrés, Chem. Phys. Lett. **288**, 299 (1998).

[24]V. Veryazov, P. O. Widmark, L. Serrano-Andrés, R. Lindh, and B. O. Roos, Int. J. Quantum Chem. **100**, 626 (2004).

[25]G. Karlström, R. Lindh, P.-Å. Malmqvist, B. O. Roos, U. Ryde, V. Veryazov, P. O. Widmark, M. Cossi, B. Schimmelpfennig, P. Neogrady, and L. Seijo, Comput. Mater. Sci. **28**, 222 (2003).

[26]F. Aquilante, L. De Vico, N. Ferre, G. Ghigo, P.-Å. Malmqvist, P. Neogrady, T. B. Pedersen, M. Pitonak, M. Reiher, B. O. Roos, L. Serrano-Andrés, M. Urban, V. Veryazov, and R. Lindh, J. Comput. Chem. **31**, 224 (2009).

[27]F. Aquilante, J. Autschbach, R. K. Carlson, L. F. Chibotaru, M. G. Delcey, L. De Vico, I. F. Galván, N. Ferré, L. M. Frutos, L. Gagliardi, M. Garavelli, A. Giussani, C. E. Hoyer, G. Li Manni, H. Lischka, D. Ma, P.-Å. Malmqvist, T. Müller, A. Nenov, M. Olivucci, T. B. Pedersen, D. Peng, F. Plasser, B. Pritchard, M. Reiher, I. Rivalta, I. Schapiro, J. Segarra-Martí, M. Stenrup, D. G. Truhlar, L. Ungur, A. Valentini, S. Vancoillie, V. Veryazov, V. P. Vysotskiy, O. Weingart, F. Zapata, and R. Lindh, J. Comput. Chem. **37**, 506 (2016).

[28]F. Weigend and R. Ahlrichs, Phys. Chem. Chem. Phys. **7**, 3297 (2005).

[29]K. A. Peterson and C. Puzzarini, Theor. Chem. Acc. **114**, 283 (2005).

[30]D. Figgen, G. Rauhut, M. Dolg, and H. Stoll, Chem. Phys. **311**, 227 (2005).

[31]K. A. Peterson, J. Chem. Phys. **119**, 11099 (2003).

[32]K. A. Peterson, D. Figgen, E. Goll, H. Stoll, and M. Dolg, J. Chem. Phys. **119**, 11113 (2003).

[33]T. Noro, M. Sekiya, and T. Koga, Theor. Chem. Acc. **131**, 1124 (2012).

[34]T. Noro, M. Sekiya, and T. Koga, Theor. Chem. Acc. **132**, 1363 (2013).

[35]B. O. Roos, R. Lindh, P.-Å. Malmqvist, V. Veryazov, and P. O. Widmark, J. Phys. Chem. A **108**, 2851 (2004).

[36]D. Andrae, U. Haussermann, M. Dolg, H. Stoll, and H. Preuss, Theor. Chim. Acta **77**, 123 (1990).

[37]M. Reiher and A. Wolf, J. Chem. Phys. **121**, 2037 (2004).

[38]M. Reiher and A. Wolf, J. Chem. Phys. **121**, 10945 (2004).

[39]D. Peng and K. Hirao, J. Chem. Phys. **130**, 044192 (2009).

[40]D. Peng and M. Reiher, Theor. Chem. Acc. **131**, 1081 (2012).

[41]K. Andersson, P.-Å. Malmqvist, B. O. Roos, A. J. Sadlej, and K. Wolinski, J. Phys. Chem. **94**, 5483 (1990).

[42]K. Andersson, P.-Å. Malmqvist, and B. O. Roos, J. Chem. Phys. **96**, 1218 (1992).

[43]G. Ghigo, B. O. Roos, and P.-Å. Malmqvist, Chem. Phys. Lett. **396**, 142 (2004).

[44]N. Forsberg and P.-Å. Malmqvist, Chem. Phys. Lett. **274**, 196 (1997).

[45]B. Schimmelpfennig, Amfi, an atomic mean-field spin-orbit integral program, Stockholm: Stockholm University, 1996.

[46]B. A. Heß, C. M. Marian, U. Wahlgren, and O. Gropen, Chem. Phys. Lett. **251**, 365 (1996).

[47]C. A. Wight, B. S. Ault, and L. Andrews, J. Mol. Spectrosc. **56**, 239 (1975).

[48]D. T. Radzykewycz, C. D. Littlejohn, M. B. Carter, J. O. Clevenger, J. H. Purvis, and J. Tellinghuisen, J. Mol. Spectrosc. **166**, 287 (1994).

[49]J. O. Clevenger, Q. P. Ray, and J. Tellinghuisen, Can. J. Phys. **72**, 1294 (1994).

[50]L. E. Selin and B. Soderborg, Ark. Fys. **21**, 515 (1962).

[51]D. Fedorov and J. Finley, Phys. Rev. A **64**, 042502 (2001).

[52]D. G. Fedorov, S. Koseki, M. W. Schmidt, and M. S. Gordon, Int. Rev. Phys. Chem. **22**, 551 (2003).

[53]L. Serrano-Andrés, M. Merchán, and R. Lindh, J. Chem. Phys. **122**, 104107 (2005).

[54]M. Hargittai, Chem. Rev. **100**, 2233 (2000).

[55]P. A. Akishin and V. P. Spiridonov, Kristallografiya **2**, 475 (1957).

[56]D. Spence, R. G. Wang, and M. A. Dillon, J. Chem. Phys. **82**, 1883 (1985).